Available online at www.sciencedirect.com
SCIENCE DIRECT®
Journal of Solid State Chemistry 178 (2005) 3074–3089
JOURNAL OF SOLID STATE CHEMISTRY
www.elsevier.com/locate/jssc

Silver-halide/organic-composite structures: Toward materials with multiple photographic functionalities

Joseph F. Bringley*, Manju Rajeswaran, Leif P. Olson, Nancy M. Liebert

Research & Development Laboratories, Eastman Kodak Company, 1999 Lake Avenue, Rochester, NY 14650-2002, USA

Received 28 April 2005; received in revised form 8 July 2005; accepted 19 July 2005
Available online 24 August 2005

Abstract

We report the synthesis and structure of the novel silver-halide-based organic–inorganic hybrids $Ag_2Br_6(PPD)_2$, $Ag_2Br_6(CD\text{-}2)_2 \cdot H_2O$, $Ag_2Br_4(TMBD)$, and $Ag_2I_6(CD\text{-}2)_2 \cdot H_2O$. 1,4-phenylenediammonium hexabromodiargentate(I) $[Ag_2Br_6(PPD)_2]$ crystals are monoclinic ($P2_1/n$), with unit-cell dimensions, $a = 10.1915(3)$ Å, $b = 7.7562(2)$ Å, $c = 12.4340(5)$ Å and $\beta = 93.109(1)^\circ$. *N*,*N*-diethyl-2-methyl-1,4-benzenediammonium hexabromodiargentate(I) monohydrate $[Ag_2Br_6(CD\text{-}2)_2 \cdot H_2O]$ crystals are monoclinic (space group $P2_1/c$) with $a = 10.8434(2)$ Å, $b = 11.4293(2)$ Å, $c = 14.3729(1)$ Å, and $\beta = 96.153(1)^\circ$. *N*,*N*,*N*′,*N*′-tetramethyl-1,4-benzenediammonium tetrabromodiargentate(I) $[Ag_2Br_4(TMBD)]$ crystals are orthorhombic (space group *Pbcn*) with $a = 17.0030(6)$ Å, $b = 6.6163(2)$ Å, and $c = 15.9762(6)$ Å. *N*,*N*-diethyl-2-methyl-1,4-benzenediammonium hexaiododiargentate(I) monohydrate, $[Ag_2I_6(CD\text{-}2)_2 \cdot H_2O]$, are monoclinic ($C2/c$), with unit-cell dimensions, $a = 21.4691(4)$ Å, $b = 12.1411(2)$ Å, $c = 14.3102(2)$ Å, and $\beta = 98.657(1)^\circ$. The novel structures are members of a class of silver-halide-based organic–inorganic hybrids based upon the assembly of $[Ag_aX_b]^{n-}$ clusters and protonated organoamines in aqueous mineral acids. The clusters display short intracluster Ag–Ag distances, and computational methods are used to evaluate intracluster Ag–Ag bonding. The diverse stoichiometries and cluster connectivities observed suggest a rich compositional and structural chemistry based upon the general assembly method. We have extended the methodology to include a silver-halide–organoamonium chemistry in which the organic moiety is chosen to serve a specific photographic function and demonstrate the first examples of such materials. The methodology allows for the direct assembly of $[Ag_aX_b]^{n-}$ clusters with commercial photographic color developer molecules, and we show that development is repressed but can later be "switched on" in a unique photographic scheme. The photographic properties of $Ag_2Br_6(PPD)_2$ are examined and show an extremely facile development rate owing to the fact that the developer molecules are within molecular proximity to the clusters. As a result of their molecular nature, we anticipate that such materials could enable conventional or completely new imaging technologies with very fast image access rates and very high resolution.

Keywords: Layer structures; Inorganic/organic composites; Photographic chemistry; Silver halide; Development; Argentophilicity

1. Introduction

Modern materials chemistry is marked by a persistent evolution toward materials of greater and greater complexity and function. Examples include nanoscale molecular assemblies [1,2], polyelectrolyte multilayer assemblies [3], composite materials [4], biomimetic materials [5] and inorganic/organic hybrids [6]. The ordered assembly of materials at the nano- and molecular scale is capable of producing materials, which can simultaneously carry multiple functionalities that can be "activate-able" with respect to a stimulus, and can be integrated at unprecedented small scales. These developments have been made possible by the revolution in thinking that led to the "bottom–up" approach to the design of devices: an approach, which imagines devices being assembled one, or several, molecules at a time,

*Corresponding author. Fax: +1 585 722 4771.
E-mail address: joseph.bringley@kodak.com (J.F. Bringley).

0022-4596/$ - see front matter © 2005 Elsevier Inc. All rights reserved.
doi:10.1016/j.jssc.2005.07.018

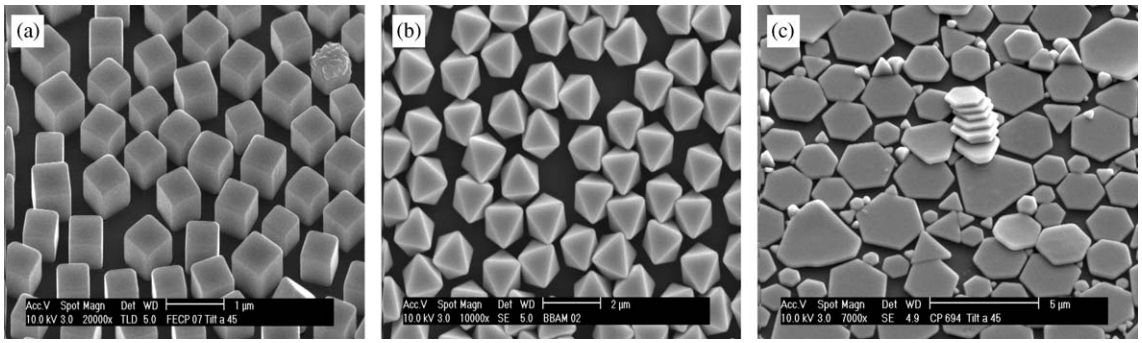

Fig. 1. SEM images showing the evolution of photographic AgX microcrystals from (a) cube-shaped, to (b) octahedrally shaped to (c) high-aspect ratio tabular crystals.

integrated at a nanoscale, and incorporating diverse sets of interacting molecules. We wish to reaffirm that photographic chemistry has long incorporated such complexities to reproduce images [7–16]. Nanoscale integration in photographic film is evidenced by a number of remarkable developments. Examples include the chemical sensitization of AgX ($X = $ Cl, Br) microcrystals [8,9], which produces nanoscale clusters at precise sites in the microcrystals [10], and spectral sensitization including the development of two-electron sensitizers [11]. The development of high-aspect ratio microcrystals [12], surface modified by the assembly of cyanine dye j-aggregates and providing spectral sensitization, is a commercial example of self-assembly of an organic phase onto an inorganic substrate [13]. The development of image formation chemistry is a remarkable example of an activated system having a chemical-feedback loop that is capable of self-inhibition [14].

One of the most well-known strategies for improving the performance of photographic AgX microcrystals is to maximize the surface-to-volume ratio of individual microcrystals [15]. This increases the number of adsorbed dye molecules per microcrystal and, hence, increases the amount of light absorption per microcrystal. Based upon this straightforward hypothesis, photographic microcrystals have undergone a continuous evolution from cube-shaped, to octahedrally shaped, to high-aspect ratio crystals, as shown in Fig. 1. Conditions have been determined [16] that favor the formation of crystals having multiple parallel twin-planes, leading to hexagonal- or triangular-shaped crystals, commonly referred to as "tabular" crystals. The dimensions of tabular crystals typically range on the order 0.5–4.0 μm in diameter (equivalent circular diameter) and 0.05–0.15 μm in thickness. To further improve light absorption per microcrystal, the photographic community continues to drive toward yet thinner tabular crystals.

In this report, we propose a synthetic methodology that, in principle, could allow photographic scientists to explore the theoretical limits of tabular grain thickness, i.e., thicknesses on the order of 10 Å. The methodology is adapted from the work of Mitzi et al. [17] and utilizes the assembly of alternating inorganic and organic frameworks via Coulomb stabilization. In this manner, pieces, or slices, of an inorganic sublattice having a net charge are stabilized by a counter-charged organic sublattice, and an alternating organic/inorganic structure is assembled. We have extended previously developed methodologies to include a silver-halide/organo chemistry in which the organic moiety is chosen to serve a specific photographic function and demonstrate the first examples of such materials. We show the direct incorporation of photographic-developer molecules into an alternating crystalline sublattice of silver-halide clusters. We describe the synthesis, structure, and photographic properties of 1,4-phenylenediammonium hexabromodiargentate(I) [$Ag_2Br_6(PPD)_2$], *N*,*N*-diethyl-2-methyl-1,4-benzenediammonium hexabromodiargentate(I) monohydrate [$Ag_2Br_6(CD\text{-}2)_2 \cdot H_2O$], *N*,*N*,*N*′,*N*′-tetramethyl-1,4-benzenediammonium tetrabromodiargentate(I) [$Ag_2Br_4(TMBD)$] and *N*,*N*-diethyl-2-methyl-1,4-benzenediammonium hexaiododiargentate(I) monohydrate, [$Ag_2I_6(CD\text{-}2)_2 \cdot H_2O$]. The goal of this research is to produce materials that possess a plurality of photographic functionalities for applications in photographic, photothermal, and other imaging or printing modalities. As a result of their molecular nature, we anticipate that such materials could enable conventional or completely new imaging technologies with very fast image access rates and very high resolution.

2. Experimental

Silver bromide was prepared by aqueous precipitation of $AgNO_3$ with NaBr and was washed with distilled water and dried. Forty-eight per cent hydrobromic acid and stabilized hydriodic acid were purchased from Aldrich Chemicals. Paraphenylenediamine (PPD), 1,4-phenylenediamine 2HCl and *N*,*N*,*N*′,*N*′-tetramethyl-1,

4-benzenediamine dihydrogen chloride were purchased from Aldrich Chemicals. *N*,*N*-diethyl-2-methyl-1,4-benzenediamine (CD-2) and AgI were obtained from Eastman Kodak Company. All operations were performed in air unless otherwise noted.

$Ag_2Br_6(CD\text{-}2)_2 \cdot H_2O$: Crystals of $Ag_2Br_6(CD\text{-}2)_2 \cdot H_2O$ suitable for single-crystal X-ray diffraction were prepared as follows: AgBr (4.00 g, 21.0 mmol) was dissolved in 50.0 mL of warm 48% hydrobromic acid and separately *N*,*N*-diethyl-2-methyl-1,4-benzenediamine hydrogen chloride (4.51 g, 21.0 mmol) was dissolved in 50 mL HBr. The two solutions were combined with stirring, heated gently to about 70 °C, and cooled slowly to 0 °C, whereupon colorless, crystalline needles formed. The needles were collected by filtration and washed with a small amount of 50:50 H_2O:HBr and dried in a desiccator under flowing nitrogen. The yield of the reaction was 5.11 g (44.8%). Elemental analysis found (calc.) gave C = 24.21% (24.33%); H = 3.61% (3.52%); N = 5.11% (5.16%); Br = 42.80% (44.15%); Ag = 20.00% (19.87%).

Ag_2Br_4(TMBD): Crystals of Ag_2Br_4(TMBD) suitable for single-crystal X-ray diffraction were prepared as follows: AgBr (4.00 g, 21.0 mmol) was dissolved in 40.0 mL, 48% hydrobromic acid and separately, *N*,*N*,*N*′,*N*′-tetramethyl-1,4-benzenediamine dihydrogen chloride (5.05 g, 21.0 mmol) was dissolved in 20 mL H_2O + 34 mL HBr. The two solutions were combined with stirring, heated gently to about 50 °C, and cooled slowly to –4 °C, whereupon colorless, crystalline needles formed. The needles were collected by filtration and washed with a small amount of 50:50 H_2O:HBr and dried in a desiccator under flowing nitrogen. The yield of the reaction was 4.12 g (54.9%). Elemental analysis found (calc.) gave C = 16.65% (17.16%); H = 2.38% (2.31%); N = 3.81% (4.02%).

$Ag_2I_6(CD\text{-}2)_2 \cdot H_2O$: Crystals of $Ag_2I_6(CD\text{-}2)_2 \cdot H_2O$ suitable for single-crystal X-ray diffraction were prepared as follows: AgI (4.00 g, 17.0 mmol) was dissolved in 20.0 mL, 57% hydriodic acid and separately, *N*,*N*-diethyl-2-methyl-1,4-benzenediamine (CD-2) (3.66 g, 17.0 mmol) was dissolved in 30 mL H_2O + 40 mL HI. The two solutions were combined with stirring, heated gently to about 40 °C, the container capped, and cooled slowly to 3 °C, whereupon colorless, crystalline needles formed. The needles were collected by filtration and washed with a small amount of 50:50 H_2O:HI and dried in a desiccator under flowing nitrogen. The yield of the reaction was 10.1 g (91.6%). Elemental analysis found (calc.) gave C = 19.31% (19.29%); H = 3.26% (2.94%); N = 4.07% (4.09%); I = 55.17% (55.59%).

$Ag_2Br_6(PPD)_2$: Crystals of $Ag_2Br_6(PPD)_2$ suitable for single-crystal X-ray diffraction were prepared as follows: AgBr (4.00 g, 21.0 mmol) was dissolved in 50.0 mL of warm 48% hydrobromic acid and separately, 1,4-benzenediamine (2.30 g, 21.0 mmol) was dissolved in a mixture of 50 mL HBr and 20 mL distilled water. The two solutions were combined with stirring, heated gently to about 70 °C, and cooled slowly to 0 °C, whereupon colorless to light-violet, crystalline needles formed. The needles were collected by filtration and washed with a small amount of 50:50 H_2O:HBr and dried in a desiccator under flowing nitrogen. The yield of the reaction was 7.92 g (81.2%). Elemental analysis found (calc.) gave C = 15.55% (15.74%); H = 2.28% (2.20%); N = 6.05% (6.11%); Br = 50.35% (52.36%); Ag = 23.06% (23.56%).

2.1. Data collection and structure determination

Single-crystal structure determination by X-ray diffraction was performed on a Nonius KappaCCD [18] or a Siemens Smart CCD diffractometer [19] equipped with a normal focus, sealed-tube X-ray source (Mo K_α radiation, $\lambda = 0.71073$ Å). Pertinent experimental details for the structure determination are presented in Table 1. The structures were solved and refined by using the SHELXTL [20] suite of programs. The hydrogen atoms were incorporated into idealized positions. Details of the final refinement are given in Table 1.

2.2. Computational methods

Calculations of the electronic structure of the silver-halide clusters were done using *Gaussian 98* (Revision A.9) [21], using crystallographically determined nuclear positions. Calculations used the B3LYP "hybrid" density functional theory (DFT) method [22] and the DFT-optimized DZVP basis set [23]. An important reason for using the all-electron DZVP basis set was to apply the atoms in molecules (AIM) methodology of Bader et al. [24] to evaluate the possibility of Ag–Ag bonding using the computed topology of the electron density. As implemented in *Gaussian 98*, AIM does not permit the use of pseudopotential basis sets. The B3LYP/DZVP method has been shown, notably by Shoeib and coworkers, to give good enthalpies for Ag-ligand complexes in a number of situations [25], and unpublished work in our laboratories has shown that geometry optimizations using this method can reasonably reproduce Ag–Ag distances found in silver carboxylate dimers. A similar use of AIM methods to evaluate Ag–Ag bonding interactions (including a description of AIM itself) has been published elsewhere [26]. In AIM, the main topological properties of the electron density $\rho(r)$ of a molecule are summarized in terms of its critical points (CPs), which represent extrema in $\rho(r)$. The CPs are defined by the curvature of $\rho(r)$ in the regions between the atomic nuclei, which as "attractors," generate local maxima in $\rho(r)$. Here we consider mostly the bond CPs (BCPs) that are found between every pair of nuclei, which are linked by a chemical bond (and are

Table 1
Summary of crystal data, data collection and refinement parameters for the structural studies of $Ag_2Br_6(CD\text{-}2)_2 \cdot H_2O$, $Ag_2Br_4(TMBD)$, $Ag_2I_6(CD\text{-}2)_2 \cdot H_2O$, and $Ag_2Br_6(PPD)_2$

Structure	$Ag_2Br_6(CD\text{-}2)_2 \cdot H_2O$	$Ag_2Br_4(TMBD)$	$Ag_2I_6(CD\text{-}2)_2 \cdot H_2O$	$Ag_2Br_6(PPD)_2$
Crystal data				
Empirical formula	$C_{11}H_{21}AgBr_3N_2O$	$C_{10}H_{16}Ag_2Br_4N_2$	$C_{11}H_{20}AgI_3N_2O$	$C_{12}H_{20}Ag_2Br_6N_4$
Formula weight (g/mol)	544.90	699.63	684.86	915.52
Temperature (K)	293(2)	293(2)	193(2)	293(2)
Wavelength (Å)	0.71073	0.71073	0.71073	0.71073
Crystal system	Monoclinic	Orthorhombic	Monoclinic	Monoclinic
Space group	*P*2(1)/*c*	*Pbcn*	C2/*c*	*P*2(1)/*n*
Unit cell dimensions				
a (Å)	10.8434(2)	17.0030(6)	21.4691(4)	10.1915(3)
b (Å)	11.4293(2)	6.6163(2)	12.1411(2)	7.7562(2)
c (Å)	14.3729(1)	15.9762(6)	14.3102(2)	12.4340(5)
α (Å)	90	90	90	90
β (Å)	96.153(1)	90	98.657(1)	93.109(1)
γ (Å)	90	90	90	90
Volume ($Å^3$)	1771.01(5)	1797.27(11)	3687.6(1)	981.4(3)
Z	4	4	8	2
Density (calc.) (Mg/m^3)	2.044	2.586	2.467	3.098
Absorption coefficient (mm^{-1})	7.898	11.058	6.109	14.215
F(000)	1044	1296	2512	848
Crystal size (mm^3)	$0.38 \times 0.34 \times 0.18$	$0.05 \times 0.17 \times 0.70$	$0.36 \times 0.24 \times 0.22$	$0.3 \times 0.06 \times 0.05$
Data collection				
Diffractometer	SMART CCD	SMART CCD	SMART CCD	KappaCCD
θ range for data collection (°)	1.89–28.32	2.40–32.56	1.92–23.26	4.73–29.76
Scan width (°)	0.3	0.3	0.3	2
Exposure time (s/frame)	10	10	10	120
Index ranges	$-14 \leqslant h \leqslant 14$	$-24 \leqslant h \leqslant 25$	$-23 \leqslant h \leqslant 20$	$-13 \leqslant h \leqslant 13$
	$-14 \leqslant k \leqslant 8$	$-9 \leqslant k \leqslant 9$	$-13 \leqslant k \leqslant 13$	$-10 \leqslant k \leqslant 10$
	$-17 \leqslant l \leqslant 18$	$-23 \leqslant l \leqslant 23$	$-15 \leqslant l \leqslant 14$	$-17 \leqslant l \leqslant 17$
Reflections collected	10229	17678	7940	16844
Independent reflections	4074	3121	2638	2429
R(int)	0.0332	0.0763	0.0225	0.1654
Completeness to $\theta = 25.00°$	98.10%	95.40%	99.20%	99.40%
Absorption correction	SADABS[a]	SADABS	SADABS	SORTAV
Refinement				
Data/restraints/parameters	4074/0/163	3121/0/85	2638/0/181	2429/0/112
Goodness-of-fit on F2	1.062	0.751	1.089	0.946
Final *R* indices $[I > 2\sigma(I)]$, R_1	0.0375	0.0346	0.0219	0.0449
wR_2	0.0847	0.0742	0.0515	0.0873
R indices (all data), R_1	0.06	0.068	0.0254	0.1145
wR_2	0.091	0.0782	0.0529	0.1063
Extinction coefficient	0.0206(6)	0.00453(15)	0.00096(3)	0.0061(6)
Largest diff. peak and hole ($e Å^{-3}$)	0.874 and −0.705	0.793 and −0.796	0.753 and −0.563	1.155 and −0.953

[a]The SADABS and SORTAV programs are based on the method of Blessing [20(b)].

absent if no chemical bond is present), and ring CPs (RCPs) that are a different class of extrema found in the interior of rings. A secondary criterion was used to evaluate the nature of the BCPs, namely the Laplacian of $\rho(r)$, $\nabla^2\rho(r)$, where a covalent bond is characterized by $(\nabla^2\rho(r) < 0)$ and a closed-shell interaction is characterized by $(\nabla^2\rho(r) > 0)$. An example of a closed-shell interaction is a hydrogen bond or an ionic bond. The computation of zero-flux surfaces for evaluating atomic charges and bond orders by Gaussian 98 generally failed and therefore are not reported.

3. Results

3.1. Synthesis and structure

$Ag_2Br_6(PPD)_2$. PPD can be considered the prototypical molecule from which all modern color photographic developers are derived. The chemistry of color photographic developers is described briefly (vide infra) and at length elsewhere [7,8]. Given sufficient time, PPD will react with AgBr, even in the absence of light or in the absence of a latent image, reducing the silver ion to a

silver metal with concomitant generation of oxidized developer. This reaction proceeds readily at high pH but is inhibited as the pH decreases. The reduction reaction must be prevented altogether at the pH of preparation (about pH 0–1) to allow for the successful synthesis of $Ag_2Br_6(PPD)_2$. The synthesis rendered clear, colorless crystals of $Ag_2Br_6(PPD)_2$, indicating the absence of oxidation of the PPD precursor, given that the oxidation product is known to be strongly violet colored. Details of the structural refinement are given in Table 1, and a view of the contents of a unit cell of the structure is given in Fig. 2. Atomic coordinates are listed in Table 2, and selected bond distances and bond angles are given in Tables 6 and 7, respectively. The structure consists of an interpenetrating lattice of silver bromide clusters and biprotonated 1,4-benzene diammonium cations. The protonation of the amine functionalities essentially prevents the reduction of the silver ions within the clusters, which would be expected for a mixture of silver bromide and "developer" at pH of about 5 or above. The silver ions are tetrahedrally coordinated by bromide ions, the tetrahedra sharing an edge with a neighboring $AgBr_4^-$ tetrahedra to produce $[Ag_2Br_6]^{4-}$ clusters. This cluster geometry appears to be quite general because it is observed in $Ag_2I_6(CD\text{-}2)_2 \cdot H_2O$, $Ag_2Br_6(CD\text{-}2)_2 \cdot H_2O$, and in $Ag_2Br_6(TMBD)_2$ (vide infra). However, the three-dimensional connectivity of the clusters can vary quite extensively. The tetrahedra are significantly distorted with tetrahedral bond angles ranging from about 90° to 130°. Upon close inspection of the geometry of the Ag_2Br_6 cluster, it is observed that the angle between the bridging bromide ions and silver Br(3)–Ag–Br(3A) is 106.66°, only slightly distorted from the ideal tetrahedral angle. The intracluster Ag–Ag distance is 3.23 Å. In related complexes, $Ag_2I_6(CD\text{-}2)_2 \cdot H_2O$, $Ag_2Br_6(CD\text{-}2)_2 \cdot H_2O$ and $Ag_2Br_6(TMBD)_2$, the intracluster Ag–Ag distances are 3.48, 2.99, and 3.31 Å, respectively, and in some cases has led us to speculate on the presence of weak Ag–Ag intracluster bonds (see Section 4). Ag–Br bonds within the polyhedra range in length from 2.59 to 2.81 Å.

Table 2
Atomic coordinates ($\times 10^4$) and equivalent isotropic displacement parameters ($Å^2 \times 10^3$) for $Ag_2Br_6(PPD)_2$

	x	y	z	U(eq)
Ag(1)	436(1)	528(1)	1226(1)	50(1)
Br(1)	−1515(1)	2504(1)	1935(1)	32(1)
Br(2)	2216(1)	−1257(1)	2336(1)	32(1)
Br(3)	730(1)	2525(1)	−421(1)	33(1)
N(1)	2599(6)	1018(7)	4653(5)	28(2)
N(2)	5311(6)	1088(8)	2007(4)	29(2)
C(1)	1011(7)	−301(9)	5710(5)	26(2)
C(2)	1252(7)	505(9)	4829(5)	22(2)
C(3)	266(8)	789(9)	4108(6)	27(2)
C(4)	5142(8)	544(9)	965(5)	26(2)
C(5)	6177(8)	−296(9)	544(5)	27(2)
C(6)	6022(8)	−827(9)	−431(6)	27(2)

U(eq) is defined as one-third of the trace of the orthogonalized U^{ij} tensor.

A polyhedral representation of the structure showing the long-range order is given in Fig. 3. In the polyhedral representation, the $AgBr_4$ tetrahedra (gray) are emphasized and the Ag atoms are not shown but reside in the center of the tetrahedra drawn. The structure is composed of alternating organic and inorganic lattices in which sheets of $[Ag_2Br_6]^{4-}$ clusters are separated by layers of PPD molecules. The PPD molecules form infinite chains oriented along the *b*-axis with an alternating orientation of the para-amino groups at very nearly 90°. The precise overlap of the benzene rings is very reminiscent of $\pi-\pi$ stacking—although the rings are not parallel—but slightly canted; the average distance between adjacent benzene rings is 3.43 Å. The structure is held together by Coulombic forces between the clusters and the biprotonated color developer molecules, and by hydrogen bonding interactions between the halides and the protonated amines. Both protonated nitrogens have five close contacts each to neighboring bromide ions, which range from 3.15 to 3.68 Å, with an average distance of 3.37 Å. These forces have been the basis of a very rich structural chemistry for metal-halide organoamines [27], and the alternating layer arrangement is a common motif among such compounds prepared to date.

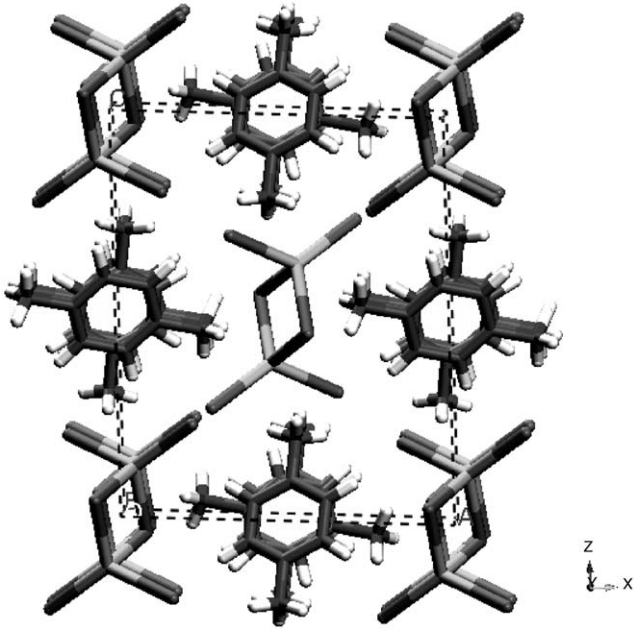

Fig. 2. A view of the unit cell of $Ag_2Br_6(PPD)_2$ perpendicular to the *ac* plane. The $[Ag_2Br_6]^{4-}$ clusters are emphasized showing the tetrahedral coordination of the silver atoms.

$Ag_2Br_6(CD\text{-}2)_2 \cdot H_2O$. *N*,*N*-diethyl-2-methyl-1,4-benzenediamine (hereafter referred to as CD-2) is a

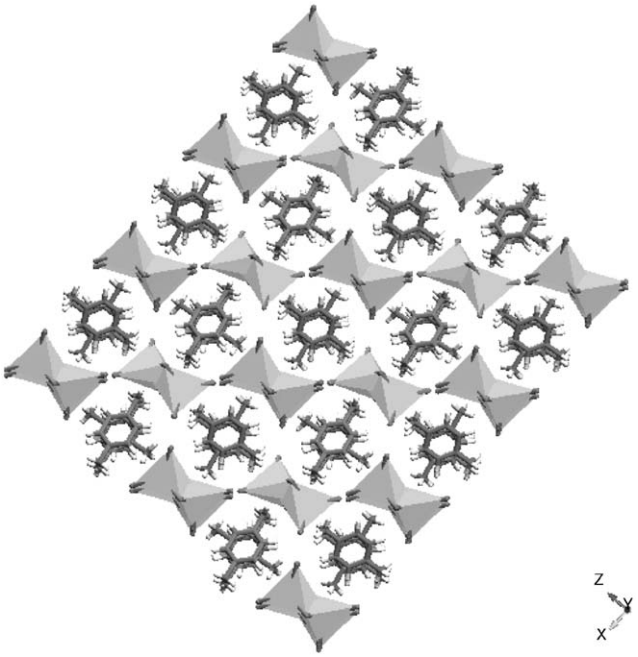

Fig. 3. Polyhedral representation of the structure of $Ag_2Br_6(PPD)_2$ showing the interpenetrating arrangement of organic and inorganic layers.

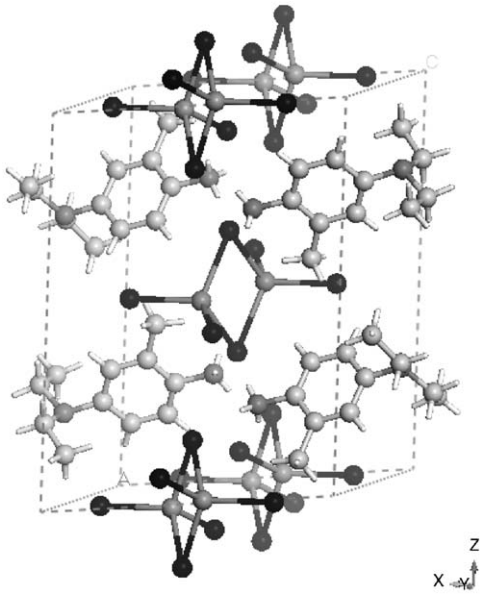

Fig. 4. A view of the unit cell of $Ag_2Br_6(CD\text{-}2)_2 \cdot H_2O$ perpendicular to the *ac* plane. The $[Ag_2Br_6]^{4-}$ clusters are emphasized showing the tetrahedral coordination of the silver atoms. Water molecules are excluded for clarity.

commercial color photographic developer. Its reaction with AgBr in hot concentrated HBr afforded colorless needles upon cooling. The structure of CD-2 is qualitatively similar to that of $Ag_2Br_6(PPD)_2$. Details of the structural refinement are given in Table 1, and a view of the contents of a unit cell of the structure is presented in Fig. 4. Atomic coordinates are listed in Table 3 and selected bond distances and bond angles are given in Tables 6 and 7, respectively. The structure consists of an interpenetrating lattice of silver bromide clusters and biprotonated color developer molecules. The silver ions are tetrahedrally coordinated by bromide ions—the tetrahedra sharing an edge with a neighboring $AgBr_4^-$ to produce $[Ag_2Br_6]^{4-}$ clusters—a nearly identical arrangement to that of $Ag_2Br_6(PPD)_2$. Ag–Br bonds within the polyhedra range in length from 2.63 to 2.82 Å. The tetrahedra are somewhat distorted with tetrahedral bond angles ranging from about 100° to 115°. This distortion gives rise to a relatively short Ag–Ag intracluster distance of 2.99 Å. This distance is only about 0.1 Å longer than the Ag–Ag distance in Ag metal (2.89 Å) and is considerably shorter than the Ag–Ag distance in AgBr, which is 4.08 Å. Upon close inspection of the geometry of the Ag_2Br_6 cluster it is observed that the angle between the bridging bromide ions and silver Br(3)–Ag–Br(3A) is 114.7°, considerably distorted from the ideal tetrahedral angle. Further, the bonds between silver and the bridging bromide ions are the longest within the tetahedra. As for $Ag_2Br_6(PPD)_2$, the structure is held together by Coulombic forces between the clusters and the biprotonated color developer molecules and by hydrogen bonding. The smallest distance from the bromide to the protonated tertiary amine nitrogen is a short 3.27 Å.

A polyhedral representation of the structure showing the long-range order is given in Fig. 5. In the polyhedral representation, the $AgBr_4$ tetrahedra are emphasized

Table 3
Atomic coordinates ($\times 10^4$) and equivalent isotropic displacement parameters ($Å^2 \times 10^3$) for $Ag_2Br_6(CD\text{-}2)_2 \cdot H_2O$

	x	*y*	*z*	*U*(eq)
Ag(1)	5805(1)	6033(1)	−136(1)	63(1)
Br(1)	8244(1)	6047(1)	16(1)	45(1)
Br(2)	4854(1)	8019(1)	−850(1)	70(1)
Br(3)	5046(1)	5560(1)	1561(1)	44(1)
O(1)	3597(4)	9550(4)	677(3)	93(1)
N(1)	3566(3)	8188(4)	2219(3)	53(1)
N(2)	−1428(3)	7813(3)	2979(3)	49(1)
C(1)	682(4)	8564(4)	3373(3)	41(1)
C(2)	1908(4)	8623(4)	3192(3)	43(1)
C(3)	2260(4)	8126(4)	2394(3)	37(1)
C(4)	1435(4)	7570(4)	1738(3)	36(1)
C(5)	1811(4)	7082(4)	842(3)	53(1)
C(6)	220(4)	7487(4)	1939(3)	41(1)
C(7)	−150(4)	7967(4)	2751(3)	38(1)
C(8)	−2396(5)	8314(6)	2265(4)	75(2)
C(9)	−2185(6)	9581(7)	2106(5)	95(2)
C(10)	−1732(5)	6519(5)	3155(4)	71(2)
C(11)	−877(7)	5993(5)	3925(6)	95(2)

U(eq) is defined as one-third of the trace of the orthogonalized U^{ij} tensor.

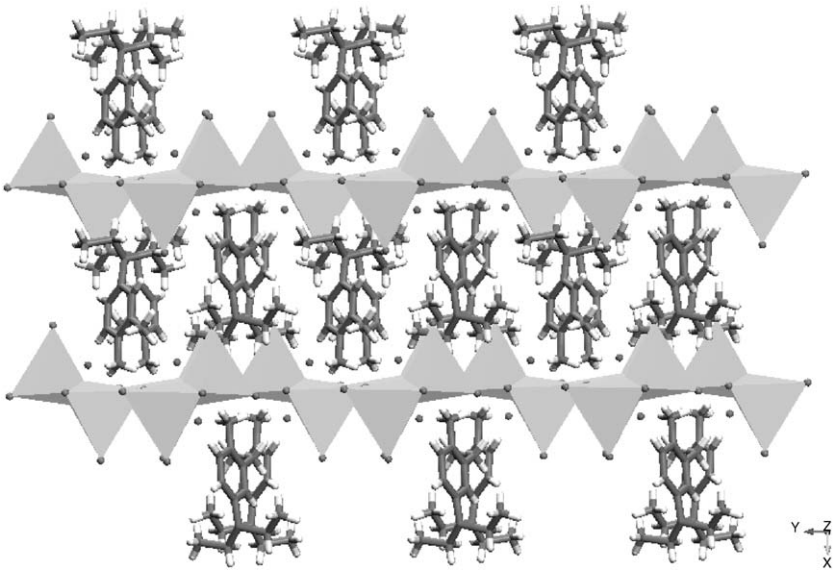

Fig. 5. Polyhedral representation of the structure of $Ag_2Br_6(CD\text{-}2)_2 \cdot H_2O$ viewed along the *c*-axis showing the interpenetrating arrangement of organic and inorganic layers.

and the Ag atoms are not shown. As is shown in Fig. 5, the structure is composed of alternating organic and inorganic lattices in which sheets of $[Ag_2Br_6]^{4-}$ clusters are separated by layers of color developer molecules. The rings of the aromatic amines are not cofacial along any crystallographic direction, presumably prevented from being so by the steric restrictions of the ethyl groups on the tertiary nitrogens. Thus, it appears that only Coulombic and hydrogen-bonding forces hold the lattice together. The primary amine of the structure has four close contacts with bromide ions, ranging from 3.27 to 4.77 Å with an average of 3.78 Å. The tertiary amine of the structure also has three close contacts with bromide ions, ranging from 3.26 to 4.69 Å, with an average of 4.19 Å. The larger average distance, when compared with that of the primary amine, is again indicative of steric constraints.

$Ag_2I_6(CD\text{-}2)_2 \cdot H_2O$: The solubility of Ag halides in aqueous mineral acids decreases along the order $AgI > AgBr > AgCl$, so the synthesis of corresponding iodide phases can be accomplished under less acidic conditions. However, the decreasing volatility of the dihalogen (I_2) and the decreasing stability of the acid increase the likelihood for impurities and inclusions contained within the crystals. Several washings were required to free the crystals of the color of iodine, and the dried crystals were unstable unless stored under dry nitrogen. Details of the structural refinement are given in Table 1, and a view of the contents of a unit cell of the structure is given in Fig. 6. Atomic coordinates are listed in Table 4 and selected bond distances and bond angles are given in Tables 6 and 7, respectively. The structure contains silver atoms tetrahedrally coordinated by iodide atoms, which are further arranged into $[Ag_2I_6]^{4-}$ polyhedra. The polyhedra are similar to those observed for the bromide phases (vide supra) but the $[Ag_2I_6]^{4-}$ clusters share alternate edges and corners to produce infinite one-dimensional chains of AgI_4 polyhedra, extending along the *c*-axis, having the overall composition

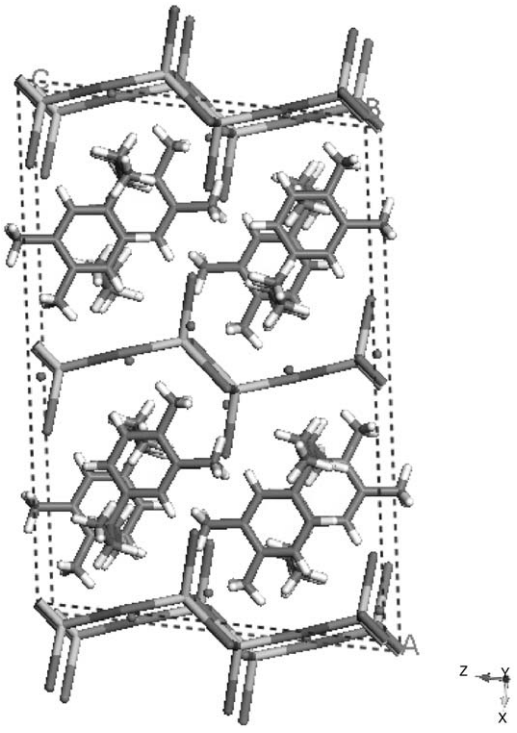

Fig. 6. A view of the unit cell of $Ag_2I_6(CD\text{-}2)_2 \cdot H_2O$ slightly canted of the *b*-axis. The connectivity of the $[Ag_2I_5]^{3-}$ chains are emphasized showing the tetrahedral coordination of the silver atoms (light gray). Water molecules are excluded for clarity.

$[Ag_2I_5]^{3-}$. The tetrahedra are somewhat distorted with relatively short Ag–Ag distances of 3.48 Å; Ag–I bonds within the polyhedra range in length from 2.81 to 2.88 Å. The CD-2 molecules occupy the interstices between the infinite chains, and the composite structure is held together by hydrogen bonds between the ammonium ions and the $[Ag_2I_5]^{3-}$ chains. In addition, the unit cell contains an iodine atom located on special positions (0, y, $\frac{3}{4}$) that is not bonded to silver (the shortest Ag–I(4) distance is 6.07 Å) but presumably shares a hydrogen bond with the primary amine of *N*,*N*-diethyl-2-methyl-1,4-benzenediamine. The distance from this iodine to the primary amine nitrogen is a short 3.63 Å.

Table 4
Atomic coordinates ($\times 10^4$) and equivalent isotropic displacement parameters ($Å^2 \times 10^3$) for $Ag_2I_6(CD\text{-}2)_2 \cdot H_2O$

	x	y	z	U(eq)
Ag(1)	4603(1)	5823(1)	5713(1)	33(1)
I(1)	5424(1)	6547(1)	4437(1)	28(1)
I(2)	5000	6826(1)	7500	25(1)
I(3)	3366(1)	6645(1)	5320(1)	31(1)
I(4)	10000	5350(1)	7500	32(1)
N(1)	9139(2)	3923(4)	9135(3)	27(1)
N(2)	6665(2)	3642(3)	7100(3)	18(1)
C(1)	7301(2)	3698(3)	7648(3)	17(1)
C(2)	7808(2)	3569(3)	7174(3)	20(1)
C(3)	8410(2)	3623(3)	7675(3)	21(1)
C(4)	8494(2)	3815(3)	8640(3)	20(1)
C(5)	7982(2)	3915(4)	9139(3)	24(1)
C(6)	7378(2)	3855(4)	8612(3)	24(1)
C(7)	6301(2)	2624(3)	7296(3)	25(1)
C(8)	6662(2)	1583(4)	7167(4)	34(1)
C(9)	6276(2)	4677(3)	7173(3)	23(1)
C(10)	6605(2)	5684(4)	6879(4)	31(1)
C(11)	8067(3)	4092(5)	10192(3)	44(1)
O(1S)	9355(2)	5804(3)	303(3)	56(1)

U(eq) is defined as one-third of the trace of the orthogonalized U^{ij} tensor.

A polyhedral representation of the structure showing the long-range order is given in Fig. 7. In the polyhedral representation, the AgI_4 tetrahedra are emphasized, and the Ag atoms are not shown. As is clear from Fig. 7, the structure is composed of alternating organic and inorganic layers, a common feature among templated structures [27]. In addition, water molecules occupy interstices between the $[Ag_2I_5]^{3-}$ chains. The *N*,*N*-diethyl substituents on the CD-2 molecules are oriented as alternating between "up" and "down" positions along both the *a*- and *b*-axes, presumably for steric reasons. Both ethyl groups are symmetrically placed above and below the plane of the phenyl ring (Fig. 6).

Ag_2Br_4(TMBD): Details of the structural refinement are given in Table 1 and a view of the contents of a unit cell of the structure is given in Fig. 8. Atomic coordinates are listed in Table 5 and selected bond distances and bond angles are given in Tables 6 and 7, respectively. The structure consists of silver atoms tetrahedrally coordinated by bromide atoms—the tetrahedra sharing *trans* edges to produce infinite one-dimensional chains of $AgBr_4$ polyhedra—extending along the *b*-axis, having the overall composition $[Ag_2Br_4]^{2-}$. The structures show a greater degree of "condensation" of the Ag-halide sublattice than either

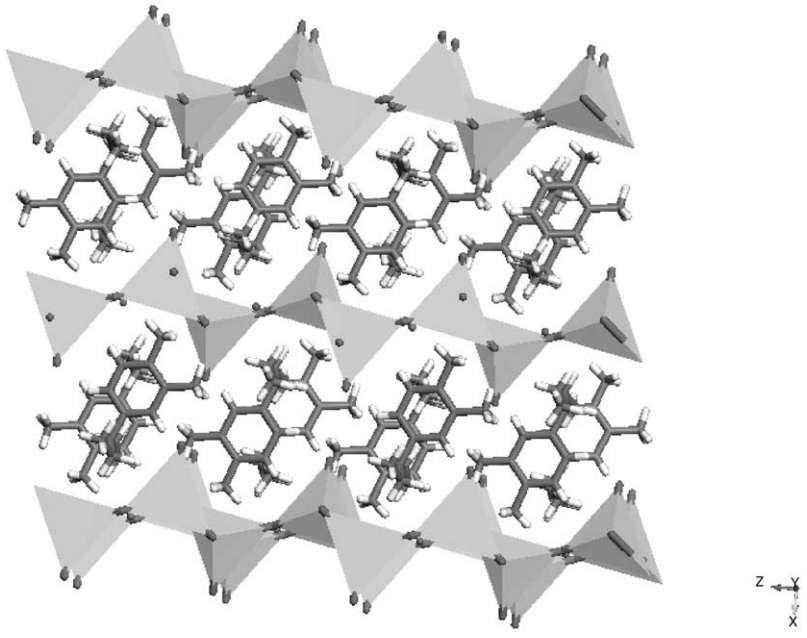

Fig. 7. Polyhedral representation of the structure of $Ag_2I_6(CD\text{-}2)_2 \cdot H_2O$ showing the alternating arrangement of organic and inorganic layers.

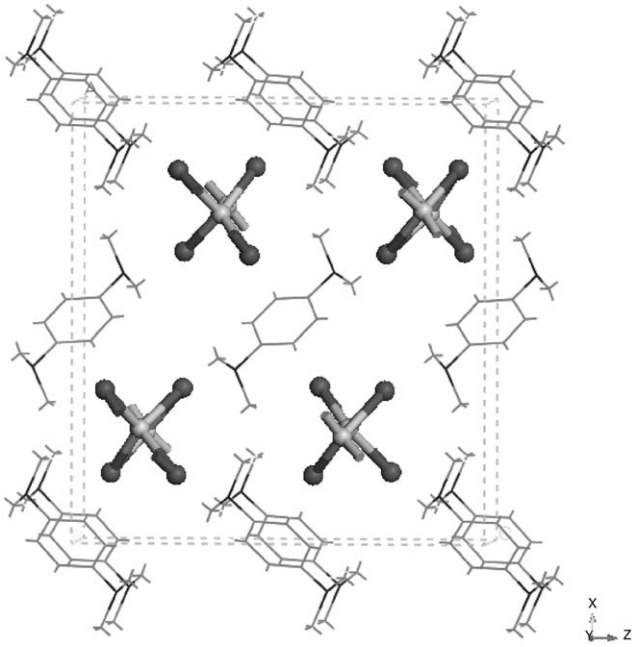

Fig. 8. A view of the unit cell of Ag_2Br_4(TMBD) canted slightly off of the *b*-axis. The infinite $[Ag_2Br_4]^{2-}$ chains are emphasized showing the tetrahedral coordination of the silver atoms.

Table 5
Atomic coordinates ($\times 10^4$) and equivalent isotropic displacement parameters ($Å^2 \times 10^3$) Ag_2Br_4(TMBD)

	x	*y*	*z*	*U*(eq)
Ag(2)	2437(1)	5759(1)	1527(1)	58(1)
Br(1)	1544(1)	3275(1)	2485(1)	50(1)
Br(2)	3473(1)	3415(1)	750(1)	53(1)
N(1)	6083(2)	1664(4)	1148(2)	44(1)
C(1)	5054(2)	−725(5)	803(2)	40(1)
C(2)	5525(2)	816(5)	541(2)	33(1)
C(3)	5480(2)	1572(5)	−256(2)	39(1)
C(4)	6884(2)	1928(7)	784(3)	79(2)
C(5)	5804(4)	3576(7)	1504(3)	100(2)

U(eq) is defined as one-third of the trace of the orthogonalized U^{ij} tensor.

of the three structures previously described, and the variation among the condensation schemes suggests a very rich structural chemistry for this relatively new class of Ag-halide compounds. The tetrahedra are somewhat distorted with tetrahedral bond angles ranging from 100° to 124°. This distortion gives rise to relatively short Ag–Ag distances of 3.31 Å, probably too long to be considered a bond but again, significantly smaller than the Ag–Ag distance in AgBr (4.08 Å). The TMBD molecules occupy the interstices between these chains, and the composite structure is held together by Coulombic forces and by hydrogen bonds between the ammonium ions and the $[Ag_2Br_4]^{2-}$ chains. The TMBD molecules form cofacial stacks along the *b*-axis but the nearest distance between two adjacent benzene rings is a long 4.89 Å. The smallest distance from bromide to the tertiary amine nitrogen is a short 3.23 Å, with four additional contact distances of 4.51, 4.59, 4.63 and 4.71 Å. Ag–Br bonds within the polyhedra range in length from 2.65 to 2.85 Å.

A polyhedral representation of the structure showing the long-range order is given in Fig. 9. In the polyhedral representation, the Ag_2Br_4 tetrahedra are emphasized and the Ag atoms are not shown. The structure is composed of interpenetrating organic and inorganic lattices. The $[Ag_2Br_4]^{2-}$ infinite chains are hexagonally packed along the *b* direction, and the amine molecules can be seen as occupying interstices between the chains.

4. Discussion

4.1. Structural design

As mentioned previously, the most common strategy for improving the performance of Ag*X* microcrystals is to maximize the surface-to-volume ratio of the individual crystallites [15]. The increasing surface area allows for greater dye adsorption (necessary for sensitization to visible light) and, concomitantly, better photon collection per crystal. This strategy has been exploited extensively to produce high-aspect ratio crystals with dimensions on the order of $4.0 \times 0.05\,\mu m$, commonly referred to as tabular crystals. Silver chloride and silver bromide are isostructural and have the simple rock-salt structure. A silver-halide tabular microcrystal is oriented with its thin axis perpendicular to the [111] direction and, thus, has two parallel [111] faces. We note that tabular crystals at their current lower limit of thickness (ca. 0.03 μm) contain about 80 AgBr layers. A view of the rock-salt structure perpendicular to the [111] axis is given in Fig. 10(a). If one theoretically takes slices of the structure perpendicular to [111], it is possible to imagine the theoretical limit to tabular grain thickness, a structure consisting of infinite $[AgBr_2]^-$ sheets that comprise silver-halide octahedra sharing trans edges. Such structure would require charge compensation by an alternating sublattice, as shown in Fig. 10(b). It is possible to imagine such an arrangement in a silver-halide structure, as depicted below, in which [1 1 1] slices of the silver-halide lattice are stabilized by alternating layers of organic cations. This strategy has been exploited by Mitzi et al. [17,27,28] to prepare a variety of alternating organic/inorganic, metal-halide perovskite-like structures. This strategy may be evolved so that the organic cation (typically an onium ion) can further carry a hydrocarbon "payload," which can be chosen to provide a specific function. Here, the term payload is used simply to mean a molecule having a particular

Table 6
Selected bond distances for $Ag_2Br_6(CD\text{-}2)_2 \cdot H_2O$, $Ag_2Br_4(TMBD)$, $Ag_2I_6(CD\text{-}2)_2 \cdot H_2O$, and $Ag_2Br_6(PPD)_2$

	$Ag_2Br_6(CD\text{-}2)_2 \cdot H_2O$	$Ag_2Br_4(TMBD)$	$Ag_2Br_6(PPD)_2$	$Ag_2I_6(CD\text{-}2)_2 \cdot H_2O$
Ag1–Ag1[a]	2.9867(8)	3.3150(1)	3.234(2)	3.4808(5)
Ag1–*X*1	2.6311(6)	2.6502(5)	2.599(1)	2.8125(5)
Ag1–*X*2	2.6535(7)	2.6546(5)	2.615(1)	2.8447(4)
Ag1–*X*3	2.7112(6)	2.7112(5)	2.696(1)	2.8616(5)
Ag1–*X*3[a]	2.8209(6)	2.8477(5)	2.809(1)	2.8852(5)

[a]Distance by symmetry transformation.

Table 7
Selected bond angles for $Ag_2Br_6(CD\text{-}2)_2 \cdot H_2O$, $Ag_2Br_4(TMBD)$, $Ag_2I_6(CD\text{-}2)_2 \cdot H_2O$, and $Ag_2Br_6(PPD)_2$

	$Ag_2Br_6(CD\text{-}2)_2 \cdot H_2O$	$Ag_2Br_4(TMBD)$	$Ag_2Br_6(PPD)_2$	$Ag_2I_6(CD\text{-}2)_2 \cdot H_2O$
X–Ag–*X*	100.83(2)	100.91(2)	90.55(4)	100.02(1)
X–Ag–*X*	108.15(2)	102.67(1)	92.14(4)	105.44(1)
X–Ag–*X*	109.039(19)	106.33(2)	106.66(4)	108.17(1)
X–Ag–*X*	111.87(2)	109.81(2)	106.89(4)	109.36(1)
X–Ag–*X*	112.07(2)	113.05(2)	128.69(4)	114.65(1)
X–Ag–*X*	114.68(2)	123.81(2)	129.13(4)	119.59(1)
X–Ag–Ag	55.57(2)	51.27(1)	50.34(3)	
X–Ag–Ag	59.12(2)	51.39(1)	56.32(3)	
X–Ag–Ag	121.23(3)	51.52(1)	106.41(4)	
X–Ag–Ag	126.18(3)	55.31(1)	120.71(4)	
X–Ag–Ag		122.72(2)		
X–Ag–Ag		122.97(1)		
X–Ag–Ag		129.87(1)		
X–Ag–Ag		134.36(2)		
Ag–*X*–Ag	65.32(2)	73.17(1)	73.34(4)	74.56(1)
Ag–*X*–Ag		77.35(1)		129.30(2)
Ag–Ag–Ag		172.64(2)		

function or property. Given that onium ions are virtually ubiquitous in photographic chemistry, the list of functional molecules can include developers, inhibitors, dyes, couplers, electron transfer agents, etc. [7,8] The strategy then, in essence, attempts to exploit structural complexity to expand the chemical and physical functionality of the system.

The idealized structure shown in Fig. 10(b) is not observed for any of the materials synthesized herein; however, we would like to point out some similarities (and dissimilarities) and further highlight the structural diversity of the compounds. The most obvious dissimilarity between the idealized structure and the reported structures is the coordination of the silver ion, which is octahedral in the idealized structure but tetrahedral in the compounds reported. Ag(I) can form compounds having a wide range of coordination numbers, generally 2, 3, 4, and 6 with halides, but also 7 and 8 in oxy compounds [29]. For halides other than simple binary compounds (X = F, Cl, and Br), coordination number 4 appears to be the most common. It has been noted that the lower the coordination number the greater the covalent character of the bond [29]. We anticipate that a higher degree of condensation of the clusters would be necessary to stabilize higher coordination geometries. The degree of condensation varies quite considerably in the compounds reported, beginning with isolated $[Ag_2Br_6]^{4-}$ clusters in $Ag_2Br_6(PPD)_2$ and $Ag_2Br_6(CD\text{-}2)_2 \cdot H_2O$, to $[Ag_2I_6]^{4-}$ clusters condensed at the apexes to form one-dimensional $[Ag_2I_5]^{3-}$ chains in $Ag_2I_6(CD\text{-}2)_2 \cdot H_2O$ and, finally, edge-condensed tetrahedra, $[Ag_2Br_4]^{2-}$ in $Ag_2Br_4(TMBD)$. The degree of condensation must depend upon a number of factors, including the charge, size, and packing constraints of the organoamine moiety, and the Coulombic periodicity established.

4.2. Electronic structure of silver-halide complex ions

We have noted that the [Ag–*X*] clusters of the compounds reported herein have short Ag–Ag contacts. For example, in $Ag_2Br_6(CD\text{-}2)_2 \cdot H_2O$, the Ag–Ag distance of 2.99 Å is only about 0.1 Å longer than the Ag–Ag distance in Ag metal (2.89 Å) and is considerably

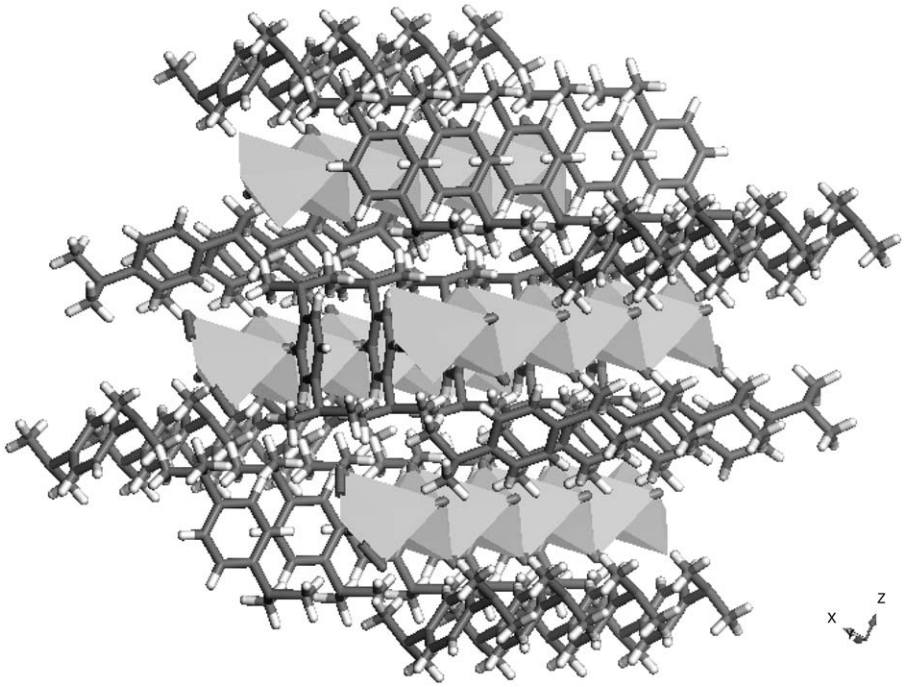

Fig. 9. Polyhedral representation of the structure of Ag_2Br_4(TMBD) showing the interpenetrating arrangement of organic and inorganic chains and the one-dimensional nature of the $[Ag_2Br_4]^{2-}$ chains.

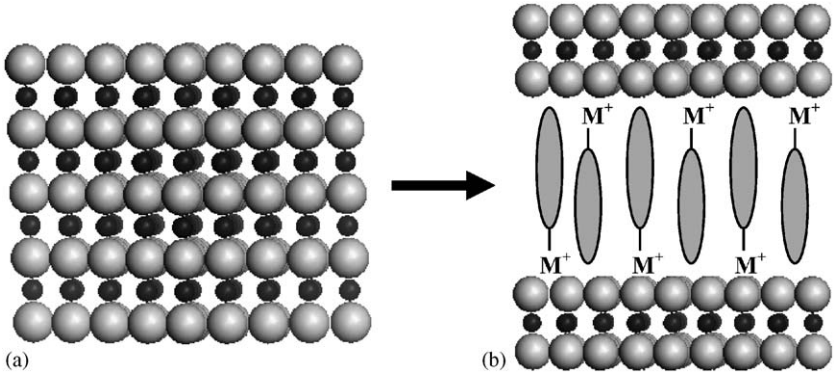

Fig. 10. (a) The AgBr structure viewed perpendicular to its [111] direction. (b) An idealized view of the structure in which "slices" comprising $[AgBr_2^-]$-infinite sheets are taken along [111]. The charge of the sublattice is compensated by organic cations (M^+) that can further carry an organic molecule chosen to provide a specific function (represented by elongated ovals).

shorter than the Ag–Ag distance in AgBr, which is 4.08 Å. Further, the angle between the bridging bromide ions and silver Br(2)–Ag–Br(2A) in the cluster is considerably distorted from the ideal tetrahedral angle, and the bonds between silver and the bridging bromide ions are the longest within the tetrahedra. All of these observations seem to indicate the existence of a metal–metal bond character within the clusters. However, this is puzzling given that $Ag_2Br_6(CD\text{-}2)_2 \cdot H_2O$ is not colored and because the stoichiometry of the material strongly suggests a cluster whose charge is $[Ag_2Br_6]^{4-}$, i.e., the charges are simply Ag^+ and Br^-. We, therefore, have examined the electronic structure of the compounds reported herein via the AIM methodology [24] to elucidate the nature of their Ag–Ag interactions. If present, an Ag(I)–Ag(I) bond is interpreted as a metallophilic d^{10}–d^{10} closed-shell attraction. Metallophilicity promotes aggregation of coinage metal (Au, Ag, Cu) centers in the +1 oxidation state, and has been studied using crystallographic, spectroscopic, and computational methods [30] The propensity for metallophilicity is, in general, Au(I) > Ag(I) > Cu(I), because of the reinforcing influence of relativistic effects [31a,c]. As a rough guide, both "aurophilic" and "argentophilic" bonds have been estimated as approximately as strong as hydrogen bonds [31].

For $Ag_2Br_6(CD\text{-}2)_2 \cdot H_2O$ and $Ag_2Br_6(PPD)_2$, the Ag–X anion for electronic structure calculations is the monomeric $[Ag_2X_6]^{4-}$ species (X = Br) shown in Scheme 1.

For the polymeric anions $([Ag_2I_5]^{3-})_n$ and $([Ag_2Br_4]^{2-})_n$ in the $Ag_2I_6(CD\text{-}2)_2 \cdot H_2O$ and $Ag_2Br_4(TMBD)$ structures, respectively, it was necessary to select representative fragments. For evaluating argentophilic bonding, a proper fragment must contain two or more silver atoms, but another issue of concern is edge effects caused by abrupt termination of the fragment at a silver atom, i.e., at a partially bare metal ion. Owing to concerns about edge effects, it was thought to be desirable (if possible) to maintain a full coordination sphere of four halide ions about the silver ions. Alternatively, a partially uncoordinated silver ion might have been used as an "end cap" to neutralize some of the negative charges. Thus, for $Ag_2I_6(CD\text{-}2)_2 \cdot H_2O$ and $Ag_2Br_4(TMBD)$, it still seemed reasonable to use $[Ag_2X_6]^{4-}$ as a starting point to model the polymeric anion, and in the case of $Ag_2Br_4(TMBD)$, additional calculations were done with two silver ions added as end caps, yielding an $[Ag_4Br_6]^{2-}$ structure.

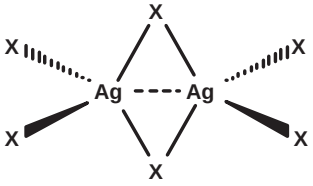

Scheme 1.

Fig. 11 shows five clusters for which AIM/B3LYP/DZVP calculations were done, e.g., one model cluster for $Ag_2Br_6(CD\text{-}2)_2 \cdot H_2O$, $Ag_2Br_6(PPD)_2$, and $Ag_2I_6(CD\text{-}2)_2 \cdot H_2O$, and two different fragments for $Ag_2Br_4(TMBD)$. The results of the AIM analysis are summarized in Table 8. Note that the only structure that contains an argentophilic bond, as determined by AIM/B3LYP/DZVP, is the $[Ag_2Br_6]^{4-}$ cluster of $Ag_2Br_6(CD\text{-}2)_2 \cdot H_2O$. This cluster has a relatively short 2.99 Å Ag–Ag distance. For the central Ag_2Br_2 unit of this cluster, a BCP is found on the attractor-interaction line between the silver ions, and two (three-membered) RCPs are found, thereby defining a fused-bicyclic ring system. As a consequence of symmetry, the BCP is

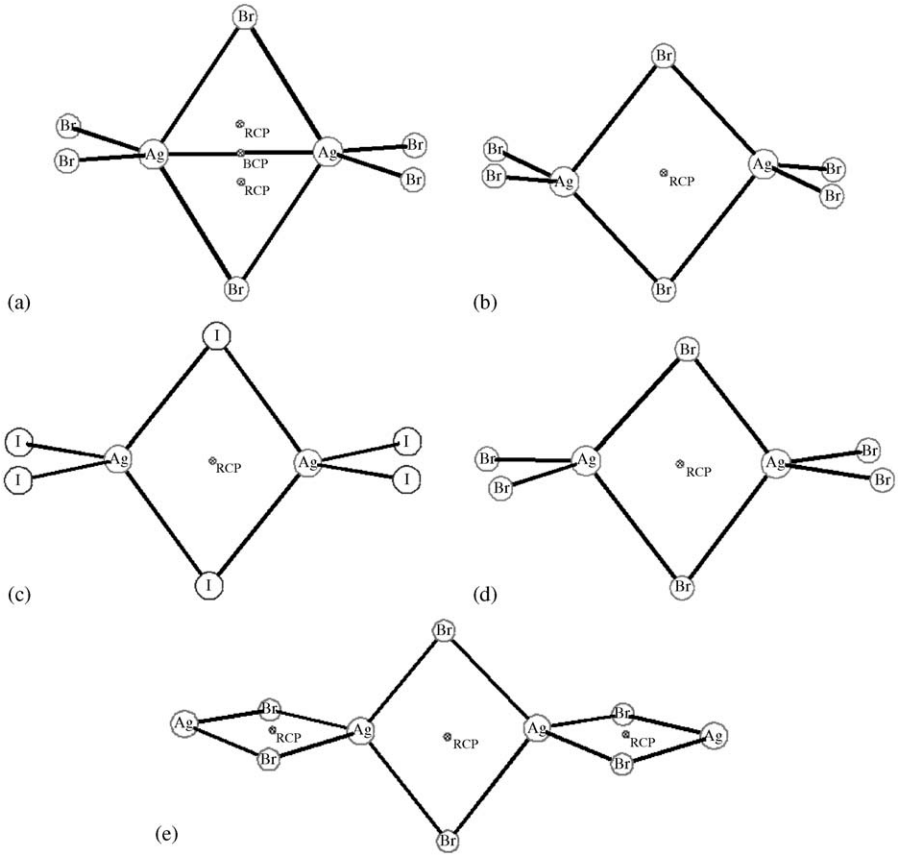

Fig. 11. Comparison of AIM/B3LYP/DZVP results for silver-halide cluster anions. Structures a–d are tetraanionic, whereas e is dianionic. Note that structure e is derived from structure d, by end capping with two Ag^+ ions, using the crystallographic positions found in the $([Ag_2Br_4]^{-2})_n$ polyanion. For clarity, the Ag–Br bond critical points are not shown. The features of interest are certainly the CPs in the Ag_2Br_2 ring systems of the clusters, as labeled in the figure. Because structure a contains an Ag–Ag BCP, there are two RCPs in this Ag_2Br_2 unit.

Table 8
Summary of the results of the AIM analysis

X-ray structure	Model cluster	Ag–Ag distance (Å)	AIM: Ag–Ag BCP present?	AIM: RCPs in central Ag_2Br_2 array
$Ag_2Br_6(CD2)_2 \cdot H_2O$	$[Ag_2Br_6]^{4-}$	2.987	Yes	2 (three-membered)
$Ag_2Br_6(PPD)_2$	$[Ag_2Br_6]^{4-}$	3.234	No	1 (four-membered)
$Ag_2I_6(CD2)_2 \cdot H_2O$	$[Ag_2I_6]^{4-}$	3.481	No	1 (four-membered)
$Ag_2Br_4(TMPD)$	$[Ag_2Br_6]^{4-}$	3.315	No	1 (four-membered)
$Ag_2Br_4(TMPD)$	$[Ag_4Br_6]^{2-}$	3.315	No	1 (four-membered)

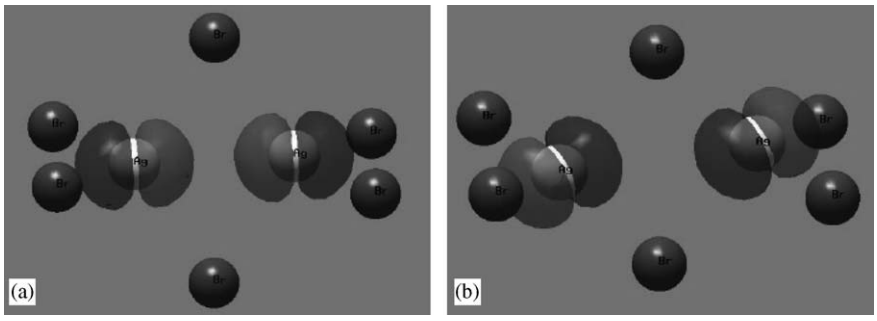

Fig. 12. Plots of orbital #115 (HOMO-39) illustrate how distortion of the $[Ag_2Br_6]^{4-}$ cluster away from idealized D_{2h} symmetry influences the directionality of the metal orbitals; in this case, the 5*p*(x) bonding combination. (This *p* orbital is shown because it is readily illustrated, but the same result is found for the *d* orbitals as well.) Note that in cluster a (from $Ag_2Br_6(CD\text{-}2)_2 \cdot H_2O$) the *p* orbitals are well-aligned, compared to cluster b (from $Ag_2Br_6(PPD)_2$), which is further distorted from D_{2h}, so there is more tilting of the orbitals. The distortion-induced misalignment of structure b can lessen the potential for Ag–Ag bonding.

exactly halfway between the silver ions, with a density Laplacian ($\nabla^2\rho(r)$) value of $+0.072$. $\nabla^2\rho(r)>0$; therefore, this is a closed-shell interaction, as expected for the interaction of two d^{10} Ag^+ ions. The remaining structures b–e in Fig. 11 have longer Ag–Ag distances, and contain (four-membered) RCPs Ag_2Br_2 rings, but no Ag–Ag BCPs. For clarity, the Ag–Br BCPs are not shown.

It was thought molecular orbital (MO) theory might explain why only one of the clusters shows Ag–Ag bonding. Examination of the fairly complicated MOs for the clusters reveals little about the ordering of MOs, or structure of the MOs, in the vicinity of the HOMO, that explains bonding. One observes many doubly occupied Ag–Ag bonding/antibonding orbitals with few obvious patterns to implicate any particular orbital(s). However, the directionality of the silver *p* and *d* orbitals is strongly influenced by the positions of the Br ligands (which, in turn, are probably influenced by crystal packing forces). For example, the $[Ag_2Br_6]^{4-}$ cluster from $Ag_2Br_6(CD\text{-}2)_2 \cdot H_2O$ is closer to ideal D_{2h} symmetry than the analogous cluster from $Ag_2Br_6(PPD)_2$, which shows more distortion of the Br ligands in the $\pm y$ and $\pm z$ directions (e.g., from the orientations shown in Fig. 11), in the latter case. Fig. 12 compares two orbitals, for which this is easily seen. Note the differences in alignment, e.g., the lobes are both parallel and (roughly) collinear in one case (Fig. 12(a)), whereas in the other case, they are parallel but not collinear. Such differences were entirely typical of the *p* and *d* orbital comparisons between these two clusters, and points to metal–metal *p* and *d* orbital alignment as a potential contributor to Ag–Ag bonding.

This orbital-directionality argument can also apply to $Ag_2Br_4(TMBD)$, where the $[Ag_2Br_6]^{4-}$ fragment has similar distortions, like that found in structure (b) of Fig. 12, which could explain the lack of Ag–Ag bonding. This argument, however, does not seem to apply to $Ag_2I_6(CD\text{-}2)_2 \cdot H_2O$, where the $[Ag_2I_6]^{4-}$ cluster is close to D_{2h} symmetry, yet no Ag–Ag bond is present. An alternative hypothesis was tested that assumed that the additional electrons in iodide might counteract Ag–Ag bonding by involving more of the Ag orbitals in Ag–I orbital overlaps. A computational experiment was done of using the X-ray coordinates of the $[Ag_2Br_6]^{4-}$ cluster with the 2.99 Å Ag–Ag distance but replacing the bromide ions with iodide to give a hypothetical $[Ag_2I_6]^{4-}$ cluster. AIM/B3LYP/DZVP analysis showed that the Ag–Ag bond was still present, eliminating the iodide-orbital hypothesis.

At present, the best explanation for the lack of Ag–Ag bonding in three of the four crystal structures is that the Ag–Ag bond is potentially present but can be nullified by subtle structural factors. This is reasonable because argentophilic bonding is considered to be a relatively weak interaction. One structural factor that might

nullify the Ag–Ag bond could be positioning of the halide ligands in such a way to cause orbital misalignments between the metal ions. In the case of iodide as a bridging ligand for two silver ions, the greater (~0.15 Å) Ag-I vs. Ag–Br distance presumably tends also to increase the Ag–Ag distance. This structural factor may make Ag–Ag bonding more difficult. While the electronic structure calculations suggest that Ag–Ag bonding interactions can exist in the [Ag–*X*] clusters, such bonding is apparently not important in driving the formation of the clusters because the intracluster Ag–Ag distance does not appear to correlate with the size or geometry of the organic moiety or with the identity of the halide or with the condensation and degree of connectivity of the clusters.

4.3. Functional design

The photographic process, in its most basic form, comprises silver halide (capable of capturing electromagnetic energy and storing it as a latent image) and developer chemistry (capable of converting the latent image to a visible image). These two chemistries, however, are incompatible, i.e., unexposed silver halide is thermodynamically unstable with respect to reduction in the presence of developer molecules. The consequence is that the photographic subsystems must be kept spatially or temporally separate, with each function performed in sequence, and thus, silver-halide photography requires multiple steps. Incorporation of development and other reactive chemistries directly into film formulations has long been a goal in the photographic industry, and is particularly important for photothermographic media [32]. Because of the inherent instabilities eluded to above, however, direct incorporation most often results in temporal instability of the film and has been, for the most part, impractical. We have attempted here to design a synthetic process whereby developer molecules are incorporated directly into the crystalline lattice of a silver-halide complex. Commercial color developer molecules are derived from paraphenylene diamine and some common developers are shown in Fig. 13. Color developer molecules are oxidized by interaction with latent image clusters on silver halide and in turn react with photographic "coupler" molecules to produce dye, i.e., color image [7]. For a detailed description of the chemistry of the development process, we refer the reader to several excellent reviews on this subject [7,8].

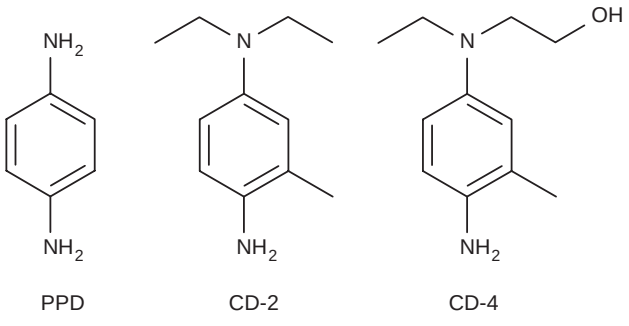

Fig. 13. Molecular structures of photographic color developers.

The synthetic methodology chosen for preparation of Ag*X*-organoamine composites was adapted from that of Mitzi et al. [17]. The method had been employed to prepare metal-halide-organoamine composites utilizing Sn, Ge, Cu, Pb, Eu, and other metals; and remarkable rich structural chemistry and diverse physical properties have been found [27]. Comparatively few Ag*X*-organoammonium complexes have been prepared and the majority of compounds reported are based upon silver-iodide, with relatively few silver-bromides reported. Mukherjee et al. [33] reported the formation of adducts of tetraethylammonium and tetrabutylammonium cations with AgBr in organic solvents. Peters et al. [34] reported the structure of $[N(CH_3)_4]AgI_2$ and Owens et al. [35] reported the formation of a series of AgI adducts having the general formula, $Ag_8I_9[N(R_4)]$. Thackeray and Coetzer [36] described the synthesis and structure of $[(CH_3)_3NCH_2CH_2N(CH_3)_3]Ag_2I_4$, a structure which contains infinite chains of edge-sharing $[Ag_2I_4]^{2-}$ tetrahedra that are similar to those reported herein for Ag_2Br_4(TMBD). Many additional silver-iodide-based organoammonium compounds have been reported including those by Geller and Owens [37] and the tetra-metal cluster reported by Estienne [38]. Perhaps the one common feature of nearly all silver-halide-based organoammonium structures is the tetrahedral coordination of the silver ions, the condensation and three-dimensional connectivities of which forms the basis of a rich diverse structural chemistry. The compounds reported herein can be considered members of this potentially large class of silver-halide-based organic–inorganic hybrids based upon the assembly of $[Ag_aX_b]^{n-}$ clusters and protonated organoamines in aqueous mineral acids.

The first step in nearly any synthetic design involves the selection of a suitable solvent. In the case of silver halide, solubility is limited to a few systems but includes some organic bases, such as dimethylformamide, sparing solubility in concentrated aqueous salt solutions, and solubility in hot, concentrated (>ca. 1 N) aqueous acids. The solubility decreases along $HI > HBr \gg HCl$, and we note that we were not successful in attempting to grow crystals from hydrochloric acid. In our case, the aqueous acid serves two additional functions. The first is to protonate the organoamine to produce a positively charged organoammonium cation, which can "assemble" with the negatively charged silver-halide sublattice (vide infra). The second is to prevent the reduction of silver halide to silver metal by the developer—or to

at least temporarily "turn off" the function of the developer molecule. The method further relies on the formation of complex heteronuclear species having the general formula $[Ag_aX_b]^{n-}$, whose negative charge drives the crystallization with the positively charged organoammonium sublattice. Complex species are known to form in aqueous salt solutions of silver halides [8].

The incorporation of developers into the structures is particularly obvious given that many are amines and can form onium ions, but it is also an especially interesting case because developers are active only at high pH ($>\sim$5) and are inactive below the pH of 2, i.e., in their fully protonated state. Thus, the assembly of the organo-inorganic hybrid structure is essentially accomplished with the developers in an "off" state. This leads to unique equilibrium chemistry that, when the title compounds are placed in water, dependent upon the pH, they can disassemble according to the equation

$$[Ag_aX_b]^{n-}[\text{R-NH}_3^+]^{n+} \rightleftarrows AgX + \text{R-NH}_2 + HX. \quad (1)$$

The disassembly at an elevated pH yields silver halide and developer in an active state and, thus, the materials are switchable with pH. The disassembly and activation may be exploited quite simply in existing photographic systems, since pH at development is typically between about 9 and 11. The equilibrium and the rate of disassembly can be controlled somewhat by choice of amine and halide. Amines which contain hydrophobic constituents and are less soluble in water will slow disassembly, and the disassembly rate will follow Cl > Br > I, i.e., the order of solubility of the silver halides. The "switch-ability" is demonstrated by the observation that gelatin suspensions of this material immediately turn black upon addition of a few drops of base and by the fact that coatings of this material may be developed imagewise (i.e., proportional to light exposure) by suspension in 5% aqueous NaOH only for 5–10 s at room temperature. Fig. 14 shows the optical density versus relative exposure for a gelatin emulsion of $Ag_2Br_6(PPD)_2$ coated onto a plastic support. The data show a typical sensitometric response as the optical density increases with increasing exposure. The light-sensitivity of the emulsion may arise in part, or entirely, from a slight "decomposition" of the compound during the preparation of the aqueous emulsion. We note that the emulsion appeared white when observed in room light, and no visual indication of AgBr (bright yellow coloration) could be ascertained. However, it seems likely that the light-sensitivity arises from the formation of a small or catalytic amount of AgBr formed in the emulsification process. This follows from the equillibrium reaction shown in Eq. (1). The light-sensitivity of the emulsion was not directly compared to that of commercial photographic emulsions but is likely at least an order of magnitude less sensitive. This would be expected because the AgX emulsion is not "chemically sensitized," as are commercial photographic emulsions. The sensitization process is known to increase sensitivity by several orders of magnitude [8].

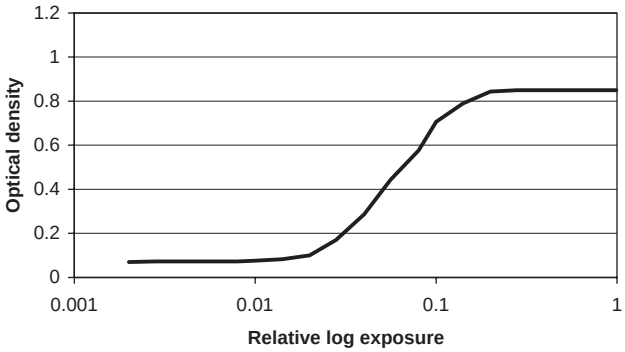

Fig. 14. The photographic response (optical density versus exposure) curve for a $Ag_2Br_6(PPD)_2$ emulsion exposed by 365 nm light. The emulsion was coated onto a plastic support in gelatin at an Ag concentration of 0.54 g/m^2 and a gelatin concentration of 2.12 g/m^2. The solids content (gelatin + $Ag_2Br_6(PPD)_2$) of the aqueous emulsion before coating was 4.51% by weight, and was blade coated with a gap of 50 μm. The emulsion was developed by immersion in 5% aqueous NaOH for 10 s, and rinsed with distilled water.

It is not clear if the intrinsic sensitivity of the emulsion as observed in this experiment is due to $Ag_2Br_6(PPD)_2$ or the formation of a small amount of AgBr that results from the equilibrium reaction given above—we note that the pH at coating was about 4.6. What is particularly remarkable, however, is the effortlessness of the development step, which occurs in less than 10 s at room temperature and probably considerably less than 5 s. Commercial photographic emulsions typically require 2–3 min at elevated temperature for complete development [8,9,15]. The facileness of the development likely is due to the fact that the PPD developer molecules are dispersed at a molecular level within the structure, and the average distance from a silver atom is only on the order of a few angstroms. Thus, diffusion to the latent image site, which is known to be a limiting step in conventional development [39], is not a limiting factor. As a result of the molecular nature of the title compounds, we anticipate that these materials could be exploited to enable conventional or completely new imaging technologies with very fast image-access rates and possibly high resolution.

Acknowledgment

Authors wish to thank Dr. Rene J. Lachicotte, University of Rochester, for data collection and structure determination for one of the complexes studied.

References

[1] A.P. Alivasatos, P.F. Barbara, A.W. Castleman, J. Chang, D.A. Dixon, M.L. Klein, G.L. McLendon, J.S. Miller, M.A. Ratner, P.J. Rossky, S.I. Stupp, M.E. Thompson, Adv. Mater. 10 (1998) 1297.

[2] G.M. Whitesides, J.C. Love, Sci. Am. 285 (2001) 39.

[3] F. Caruso, Adv. Mater. 13 (2001) 11.

[4] G. Alberti, T. Bein (Eds.), Comprehensive Supramolecular Chemistry, Solid State Supramolecular Chemistry: Two- and Three-dimensional Inorganic Networks, Elsevier, New York, 1996.

[5] N. Nandi, D. Vollhardt, Chem. Rev. 103 (2003) 4033.

[6] J.F. Bringley, N.B. Liebert, J. Disper. Sci. Technol. 24 (2003) 589.

[7] L.E. Friedrich, J.A. Kapecki, Color forming photographic materials, in: A.S. Diamond, D.S. Weiss (Eds.), Handbook of Imaging Materials, Marcel Dekker, Inc., New York, 2001, pp. 35–62.

[8] D.M. Sturmer, D.W. Heseltine, in: T.H. James (Ed.), The Theory of the Photographic Process, fourth ed., Eastman Kodak Company, Rochester, NY, 1977.

[9] T. Tani, T. Suzumoto, K. Ohzeki, J. Phys. Chem. 94 (1990) 1298.

[10] J.E. Maskasky, J. Imaging Sci. 32 (1988) 160.

[11] I.R. Gould, J.R. Lenhard, A.A. Muenter, S.A. Godleski, S. Farid, J. Am. Chem. Soc. 122 (2000) 11934.

[12] J.E. Maskasky, J. Imaging Sci. 31 (1987) 15.

[13] H.A. Herz, Adv. Colloid Interface Sci. 8 (1977) 237.

[14] N.E. Milner, J. Chem. Soc. 253 (1991).

[15] (a) J.F. Hamilton, Adv. Phys. 37 (1988) 359;
(b) A.P. Marchetti, R.S. Eachus, Adv. Photophys. 17 (1992) 145.

[16] R.W. Berriman, A.H. Herz, Nature 180 (1957) 293.

[17] D. Mitzi, S. Wang, C.A. Field, C.A. Chess, A.M. Guloy, Science 267 (1995) 1473.

[18] Nonius, KappaCCD, Nonius, Delft, The Netherlands, 2001.

[19] Bruker, SMART, Bruker-AXS Inc., Madison, USA, 2000.

[20] (a) SHELXTL: Structure Analysis software package, version 6.10, Bruker Analytical X-ray systems, Madison, WI, 2003;
(b) R.H. Blessing, Acta Crystallogr. A 51 (1995) 33.

[21] M.J. Frisch, G.W. Trucks, H.B. Schlegel, G.E. Scuseria, M.A. Robb, J.R. Cheeseman, V.G. Zakrzewski, J.A. Montgomery Jr., R.E. Stratmann, J.C. Burant, S. Dapprich, J.M. Millam, A.D. Daniels, K.N. Kudin, M.C. Strain, O. Farkas, J. Tomasi, V. Barone, M. Cossi, R. Cammi, B. Mennucci, C. Pomelli, C. Adamo, S. Clifford, J. Ochterski, G.A. Petersson, P.Y. Ayala, Q. Cui, K. Morokuma, D.K. Malick, A.D. Rabuck, K. Raghavachari, J.B. Foresman, J. Cioslowski, J.V. Ortiz, A.G. Baboul, B.B. Stefanov, G. Liu, A. Liashenko, P. Piskorz, I. Komaromi, R. Gomperts, R.L. Martin, D.J. Fox, T. Keith, M.A. Al-Laham, C.Y. Peng, A. Nanayakkara, C. Gonzalez, M. Challacombe, P.M.W. Gill, B.G. Johnson, W. Chen, M.W. Wong, J.L. Andres, M. Head-Gordon, E.S. Replogle, J.A. Pople, Gaussian 98 (Revision A.9), Gaussian Inc, Pittsburgh, PA, 1998.

[22] (a) A.D. Becke, Phys. Rev. A 38 (1988) 3089;
(b) A.D. Becke, J. Chem. Phys. 98 (1993) 5648.

[23] N. Godbout, D.R. Salahub, J. Andzelm, E. Wimmer, Can. J. Chem. 70 (1992) 560.

[24] R.F.W. Bader, Chem. Rev. 91 (1991) 893.

[25] (a) H. El Aribi, T. Shoeib, C.F. Rodriquez, A.C. Hopkinson, K.W.M. Siu, J. Phys. Chem. A 106 (2002) 2908 and references therein;
(b) A.J. Clarke, M.J. Ingleson, G. Kociok-Kohn, M.F. Mahon, N.J. Patmore, J.P. Rourke, G.D. Ruggiero, A.S. Weller, J. Am. Chem. Soc. 126 (2004) 1503.

[26] J. El-Bahraoui, J.M. Molina, D.P. Olea, J. Phys. Chem. A 102 (1998) 2443.

[27] D.B. Mitzi, Prog. Inorg. Chem. 48 (1999) 1.

[28] (a) D.B. Mitzi, K. Liang, J. Solid State Chem. 134 (1997) 376;
(b) D.B. Mitzi, Inorg. Chem. 39 (2000) 6107;
(c) D.B. Mitzi, Chem. Mater. 8 (1996) 791;
(d) D.B. Mitzi, Inorg. Chem. 35 (1996) 7614;
(e) D.B. Mitzi, K. Liang, Inorg. Chem. 37 (1998) 321.

[29] A.F. Wells, in: Structural Inorganic Chemistry, fifth ed., Clarendon Press, Oxford, 1984, p. 1098.

[30] (a) P. Pyykkö, Chem. Rev. 97 (1997) 597;
(b) S.S. Pathenini, C.J. Desiraju, J. Chem. Soc. Dalton Trans. 2 (1993) 319;
(c) N. Runeberg, M. Schutz, H.-J. Werner, J. Chem. Phys. 110 (1999) 7210;
(d) G.-C. Guo, T.C.W. Mak, Angew. Chem. Int. Ed. Engl. 37 (1998) 3183;
(e) M.A. Rawashdeh-Omary, M.A. Omary, H.H. Patterson, J. Am. Chem. Soc. 122 (2000) 10371;
(f) M.A. Omary, T.R. Webb, Z. Assefa, G.E. Shankle, H.H. Patterson, Inorg. Chem. 37 (1998) 1380;
(g) D. Perreault, M. Drouin, A. Michel, V.M. Miskowski, W.P. Schaefer, P.D. Harvey, Inorg. Chem. 31 (1992) 695;
(h) Q.-M. Wang, T.C.W. Mak, Chem. Commun. (2001) 807.

[31] A. Codina, E.J. Fernandez, P.G. Jones, A. Laguna, J.M. Lopez-de-Luzuriaga, M. Monge, M.E. Olmos, J. Perez, M.A. Rodriguez, J. Am. Chem. Soc. 124 (2002) 6781.

[32] J.M. Sturge (Ed.), Imaging Processes and Materials, Neblettes 8th ed., Van Nostran Reinhold, New York, 1989.

[33] L.M. Mukherjee, J.D. Czaban, R.S. Schultz, R.W. Atwell, R.J. Krohn, J. Inorg. Nucl. Chem. 34 (1972) 3944.

[34] K. Peters, H.G. von Schnering, W. Ott, H.-M. Seidenspinner, Acta. Crystallogr. C 40 (1984) 789.

[35] B. Owens, US Patent No. 3,541,124.

[36] M.M. Thackeray, J. Coetzer, Acta Crystallogr. B 31 (1975) 2341.

[37] S. Geller, B.B. Owens, J. Phys. Chem. Solids 33 (1972) 1241.

[38] P.J. Estienne, Acta Crystallogr. C 42 (1986) 1512.

[39] T.H. James (Ed.), The Theory of the Photographic Process, fourth ed., Eastman Kodak Company, Rochester, NY, 1977.